Final Report

For Project under

AWARD NO. FA4869-06-1-0035

by

Dr Xiaoping Li, PI of Project
Professor and Director
Neurosensors Laboratory
Department of Mechanical Engineering
National University of Singapore
Singapore 119260

Report Documentation Page

Form Approved
OMB No. 0704-0188

Public reporting burden for the collection of information is estimated to average 1 hour per response, including the time for reviewing instructions, searching existing data sources, gathering and maintaining the data needed, and completing and reviewing the collection of information. Send comments regarding this burden estimate or any other aspect of this collection of information, including suggestions for reducing this burden, to Washington Headquarters Services, Directorate for Information Operations and Reports, 1215 Jefferson Davis Highway, Suite 1204, Arlington VA 22202-4302. Respondents should be aware that notwithstanding any other provision of law, no person shall be subject to a penalty for failing to comply with a collection of information if it does not display a currently valid OMB control number.

1. REPORT DATE	2. REPORT TYPE	3. DATES COVERED
20 NOV 2007		

4. TITLE AND SUBTITLE	5a. CONTRACT NUMBER
Design and development of a super permeability nanostructured permalloy composite	5b. GRANT NUMBER
	5c. PROGRAM ELEMENT NUMBER
6. AUTHOR(S)	5d. PROJECT NUMBER
Xiaoping Li	5e. TASK NUMBER
	5f. WORK UNIT NUMBER
7. PERFORMING ORGANIZATION NAME(S) AND ADDRESS(ES)	8. PERFORMING ORGANIZATION REPORT NUMBER
National University of Singapore,10 kent Ridge Crescent,Singapore 119260,Singapore,SG,119260	**N/A**
9. SPONSORING/MONITORING AGENCY NAME(S) AND ADDRESS(ES)	10. SPONSOR/MONITOR'S ACRONYM(S)
	11. SPONSOR/MONITOR'S REPORT NUMBER(S)

12. DISTRIBUTION/AVAILABILITY STATEMENT

Approved for public release; distribution unlimited.

13. SUPPLEMENTARY NOTES

14. ABSTRACT

Theoretical analysis and modeling have been made on the magnetic behavior of ferromagnetic nanowire arrays. The design guidelines for composite ferromagnetic functional materials have been developed. The ferromagnetic functional materials should be insulated to increase sensitivity. In addition, its effective volume was studied to maximize ferromagnetism sensitivity based on the number of nanowire arrays. The dynamic domain unification principle dictated the ferromagnetic wires need to be in the array format and need to be as closely as possible each other to maximize the sensitivity.

15. SUBJECT TERMS

16. SECURITY CLASSIFICATION OF:			17. LIMITATION OF ABSTRACT	18. NUMBER OF PAGES	19a. NAME OF RESPONSIBLE PERSON
a. REPORT	b. ABSTRACT	c. THIS PAGE			
unclassified	**unclassified**	**unclassified**		**46**	

Table of Contents

1. Background Information

In the development of weak field magnetic sensors, extremely high permeability magnetic materials are essential as sensing elements. Fabrication parameters have been found to severely affect the permeability of the magnetic material, which in turn greatly affects the performance of the magnetic material as sensing elements. In chemical electrodeposition, current density[1], pH value[2], plating time[3] and the presence of seed layers[4] have been found to exert a strong influence of the composition and microstructure of the deposited layer and this in turn affects the permeability of the magnetic material. In this project, Ni-Fe was selected as the material under study due to its high initial permeability as well as near-zero magnetostriction. In sputtering, the base sputtering pressure and the substrate temperature have been reported to exert influence on the properties of the deposited material. Although much work could be done to improve existing materials by optimizing the process parameters, it appears to have reached a near limit.

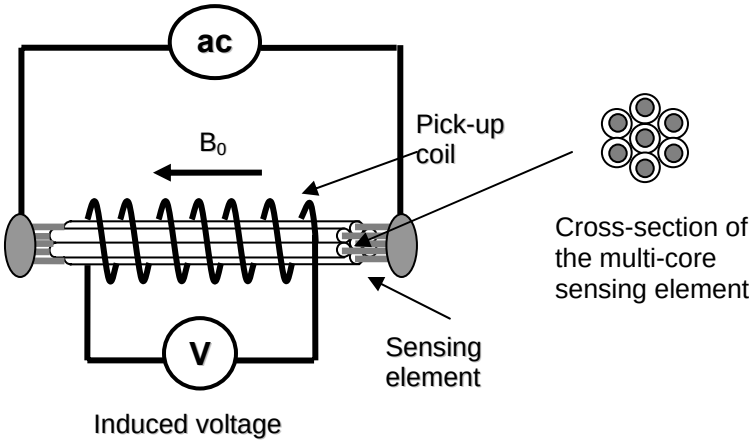

Fig. 1. Schematic of a multi-core orthogonal fluxgate sensor, in which each wire core consisted of a 16 μm diameter amorphous wire coated with a 2 μm thick glass isolation layer.

Recently, it was reported that by "packing" multiple sensing elements together (in parallel and with insulation in between the individual elements), the sensitivity of the orthogonal fluxgate sensor (Fig. 1) was observed to increase exponentially with increasing number of wires, regardless of the cross-section area of the individual wires[5].

Such sensitivity increase was neither solely due to an increase in the excitation current through cores, nor due to the increase of the volume of ferromagnetic material in the sensing element. The results further showed that there was a sensitivity resonance of the sensing element, with the resonant frequency varied with external magnetic field. All the results pointed to a conclusion that there is a dynamic magnetic interactive effect between the ferromagnetic cores in the sensing element, with which the permeability of the sensing element increases greatly with increasing number of cores in the sensing element (see Fig.2).

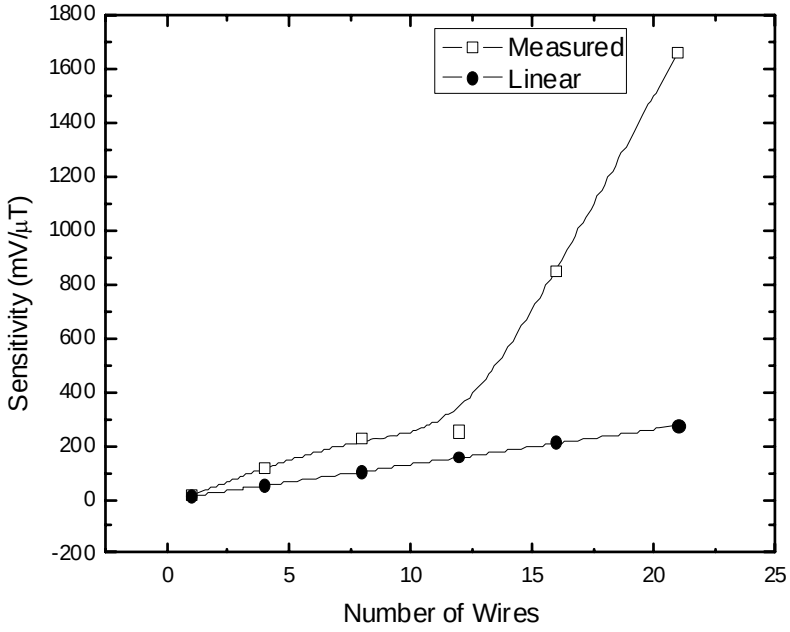

Fig. 2. Measured sensitivity increased exponentially with the number of ferromagnetic core wires increased from 1 to 21, where the "linear" curve was calculated by multiplying the number of single-core sensors and the sensitivity of a single-core sensor.

Based on the occurrence of the phenomenon of magnetic interaction between magnetic bodies as well as the obtained experimental results, showing the trend of sensitivity increasing exponentially with the number of ferromagnetic cores in the sensing element (which indicates the increase of the permeability of the sensing element

material with the number of cores in the sensing element), it is evident that in order to further increase the sensor sensitivity (besides improving the sensing element material), the number of ferromagnetic cores in the sensing element will be expected to be further increased, up to a limit such that the cross-section area of each of the ferromagnetic cores allows for the minimum requirement of alternating current passing through.

Thus, the objective of this project is to develop a nanotechnology for creating new functional materials, in which a new composite ferromagnetic material is created by packing together the insulated nanoscale stripes/wires of a ferromagnetic material for greatly enhanced magnetic permeability. In this project, firstly theoretical analyses and modeling of the magnetic behavior of in ferromagnetic wire array were made to provide the scientific basis and guidelines for the design and development of the composite ferromagnetic materials, and then the composite ferromagnetic materials were in three approaches: 1) template assisted electrodeposition; 2) combinations of lithography and sputtering; 3) simultaneous electrodeposition for Insulator/$Ni_{80}Fe_{20}$/Cu/$Ni_{80}Fe_{20}$/Insulator multiple composite wires structure.

2. Theoretical analyses and modeling of the magnetic behavior of in ferromagnetic wire array

For the scientific basis and guidelines in the design and development of the composite ferromagnetic functional materials, a hybrid theoretical model for ferromagnetic wires array are proposed based on two hypotheses: 1) the effective volume of the material increases linearly with the increase of the number of wires; 2) dynamic domain unification occurs in the ferromagnetic wire array, which greatly enhances the magnetic permeability of the material.

2.1 Effective volume

The effective volume of the material in a magnetic sensing element is the volume of the material that can be fully magnetized by the excitation field. The excitation field is

induced by the high frequency AC passing through sensing element. As the current distributes only on the surface portion of the material, which is the so-called eddy current effect, only a small portion of the material is effective for sensing. However, in case of sensing element formed by a ferromagnetic wire array with insulation between the wires, the volume of this effective portion of the sensing element material is determined by the skin depth

$$\delta = \sqrt{\frac{2}{\omega\sigma\mu}} \tag{1}$$

where ω is the angular frequency, σ is the conductivity, and μ is the maximum differential circumferential permeability of the wire.

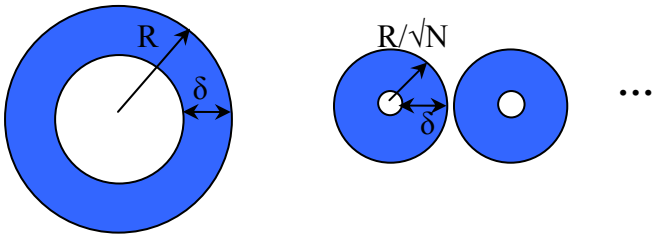

Fig. 3 Cross-sections of a single wire and an N-wire array. The blue areas represent the effective volumes of the wires.

Consider a single wire and an N-wire array with same total volume, V. The radii of the single wire and each wire in the array are R and $R/\sqrt{N}$, respectively, as shown in Fig. 3. With an arbitrary δ (δ < R), the effective volume of the single wire is

$$V - \pi(R-\delta)^2 \tag{2}$$

which is always smaller than that of the array,

$$V - N\pi(R/\sqrt{N} - \delta)^2 \tag{3}$$

With increase of N, once it satisfies

$$\delta \geq R/\sqrt{N} \tag{4}$$

or

$$N \geq (R/\delta)^2 \tag{5}$$

the total volume of the N-wire array can be the effective volume for the sensing performance to reach the optimum.

Obviously, for ferromagnetic wires array without total volume limit, the effective volume is proportional to the number of wires. As a deduction, the sensitivity of multi-core orthogonal fluxgate sensor would increase at least linearly with the increase of the number of wire cores in the sensing element.

Further, according to our experimental results, which showed that the sensitivity of multi-core orthogonal fluxgate actually increase exponentially against the number of wire cores of the sensing element, there must be other effect of the high frequency AC passing through the ferromagnetic wire array, which causes nonlinear variation of the sensitivity in relation to the number of wires in the array. This is analyzed in the next section.

2.2 Dynamic Domain Unification

Experimental results showed that the sensitivity multi-core fluxgate sensor increases with the increase of the number of wire cores occurs under following conditions:

1) the ferromagnetic wires are packed together closely to form an array;
2) all of the ferromagnetic wires have to be excited by an AC current of large enough amplitude;
3) the frequency of AC current is specified according to the number of wires.

Therefore, it can be assumed that the nonlinear effect is a short-ranged, field-induced, and frequency-dependent phenomenon, resulted from the domain interaction between wires. Based on this understanding, a dynamic domain unification model can be proposed as the following:

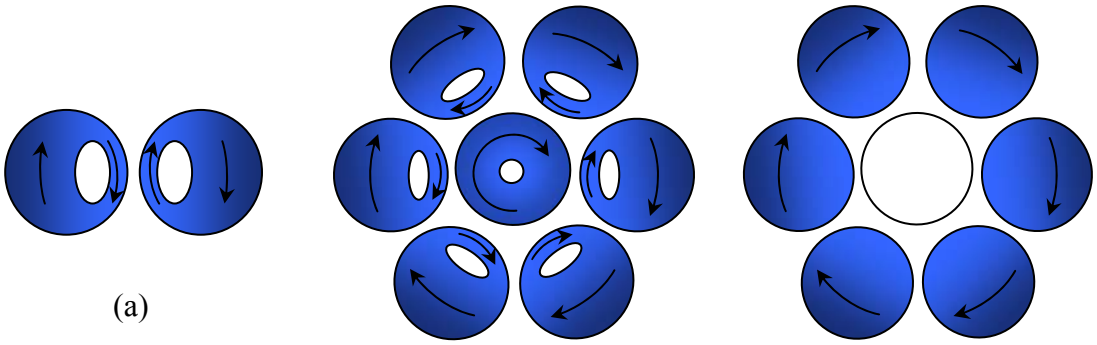

Fig. 4 Domain structure of ferromagnetic wire arrays: (a) two wires, (b) multiple wires with sandwich structure, excited at dynamic domain unification frequency and (c) multiple wires with only outer-domain unification, excited at enough high frequency

Consider a two-wire system, as shown in Fig. 2 (a). Due to the current-induced field by the neighbor wire, the current distribution will be changed. Simultaneously, the domain structure of the wire will be distorted: the size of outer parts will be enlarged and the inner parts will be reduced. For a large number of wires, the domains of neighboring wires would be "unified" and form a effective large circular domain, as shown in Fig. 4 (b). The outer part of the domains and the middle domains unify and form a domain coupling in opposite direction. The inner part domain is in the same direction as that of the outer part.

This sandwich structure is advantageous in stability, since the total magnetic energy of the coupling domains is smaller than a single domain. Note that in this structure all of the wires have AC current passing through so that they are all excited. The effective volume will not be reduced. Since large parts of the domains are unified, the total material is more uniformed, and the magnetic permeability is thus greatly enhanced.

It should be noted that the sensitivity of unified domain structure is frequency dependent. The optimum sensitivity can be obtained when the dynamic permeability is the optimum. The dynamic permeability is determined by the domain dynamics in the magnetization process, and the size and distribution of domains rely on the skin depth which is frequency dependent. This optimum frequency is the dynamic unification frequency, at which the wire array shows the sandwich structure, as seen in Fig. 2 (b).

As an extreme case, when the excitation frequency is too high, the skin depth becomes smaller such that the sandwich domain structure will disappear and only the outer-most part domains will unify, as shown in Fig. 2 (c). In this case the effective volume will be greatly reduced and the sensor sensitivity would drop.

2.3 Principles for design and application of function ferromagnetic materials based on the magnetic behavior of ferromagnetic wire array

According to the effective volume and dynamic domain unification analysis and modeling, principles and guidelines for the design and development of the composite ferromagnetic functional materials can be established.

1) For the maximum effective volume, the ferromagnetic wire array in a certain amount of materials, the number of wires should be as many as possible – leading to the requirement of nanoscaled wires.
2) For the maximum dynamic domain unification, the ferromagnetic wires in the array should be intimately close to each other with insulation in between – leading to the requirement of nanoscaled array structure.
3) In application, these function ferromagnetic materials have to be alternatively excited at a dynamic domain unification frequency for the maximum magnetic permeability.

3. Design, development and characterization of a nanoscale stripe structured Insulator/$Ni_{80}Fe_{20}$/Insulator material

3.1 Methodology

In order to obtain the multi-core structures, the general steps of fabrication and characterization have been considered and proposed, as shown in Fig. 5. A mask/template was designed and fabricated. The design of the mask/template will be shown in the later sections. Using the mask/template, deposition of the ferromagnetic material was then carried out. Depending on the suitability of the mask/template, the mask/template was removed after the deposition process. The deposited materials and their magnetic properties was then characterized accordingly.

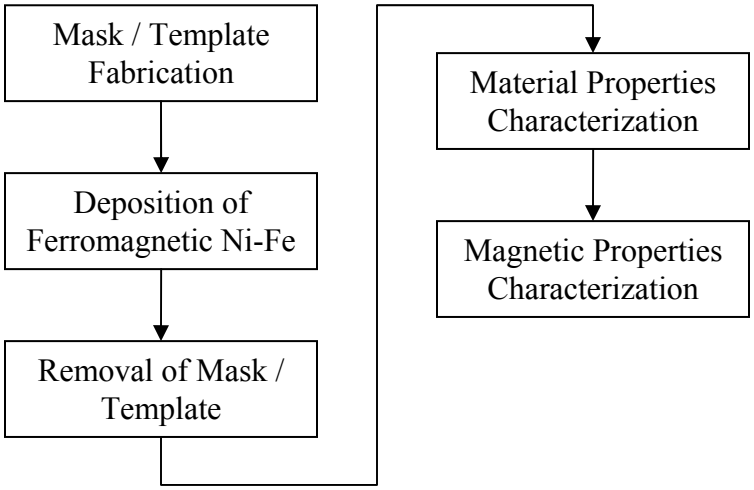

Fig. 5. Flowchart showing general steps in fabrication and characterization in order to achieve the desired multi-core structures.

Fig. 6 shows the various steps in the fabrication process that utilizes a combination of lithography and sputtering. The details of each of the steps are described as follows.

a) *Spin Coating* - The glass substrate was cleansed using alcohol and dried using nitrogen gas. A layer of SU-8 of a few microns thick as then spin coated onto the glass substrate.

b) *Exposure* - The Su-8 layer was then exposed to UV beams under a (transparency) mask to cross-link portions of the SU-8 layer.

c) *Developing* – The exposed SU-8 layer was then developed in the commercially available developer solution to obtain the template.

d) *Sputtering* – The structures were then placed in a sputtering chamber where a layer of Ni-Fe was then sputtered onto the entire structure.

e) *Removal* – The undesired Ni-Fe deposited on top of the Su-8 layer was then removed using the commercially available remover, leaving the Ni-Fe (deposited straight on the glass structure) on the glass substrate.

f) *Insulation* – In order to minimize oxidation, especially over long period of time, a layer of insulating material can be applied on top of the obtained structure.

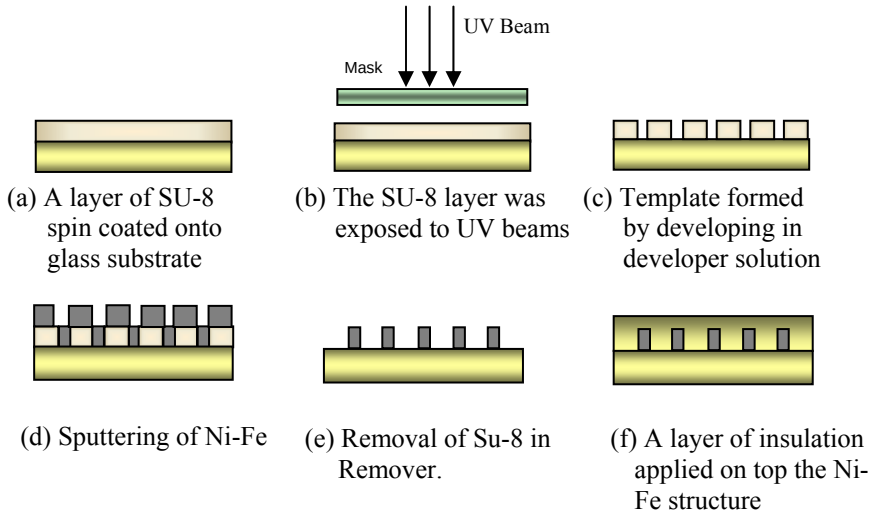

Fig. 6. Summary of the fabrication process in a combination of lithography and sputtering.

3.2 Results and Discussion

The glass substrates were firstly cleaned using an ultrasound cleaning device with acetone for 15 mins, then with IPA for 15 mins, and then with distilled water for 1 min.

The glass substrates were then dehydrated initially at 65°C for 25 mins, then at 200°C for 5 mins, and then finally maintained at a low temperature of 60°C. A layer of Su-8 2002 was then applied onto the glass substrates. The coatings were then spun at 500 rpm for 5 sec and then at 2000 rpm for 30 sec to obtain a coating layer of thickness 2 μm. The soft bake process was then carried out at 65°C for 1 min and then 95°C for 2 mins and then cooled to room temperature. The coatings were then exposed to UV light source (360-450 nm @ 4.3 MW/cm^{2}s) for 20 sec under a transparency mask (Fig. 7). The mask contained designs with varying width of the $Ni_{80}Fe_{20}$ stripes and also varying inter-distance between the stripes. The exposed coatings were then post baked for 1 min at 65°C and then at 95°C for 1 min. The designs were then obtained by placing the coatings in developed solution. The glass substrates (along with the Su-8 patterns) were then placed in a sputtering machine and a layer of $Ni_{80}Fe_{20}$ was then sputtered onto the patterns. The RF sputtering power used was 150 W and the sputtering time was 10 mins to obtain a layer of $Ni_{80}Fe_{20}$ at thickness 200 nm. The sputtering base pressure was at 10^{-6} Torr. The specimens were then placed in stripper/removal solutions to remove the cured Su-8 (with sputtered $Ni_{80}Fe_{20}$ on top) to obtain the required structures (Fig. 8).

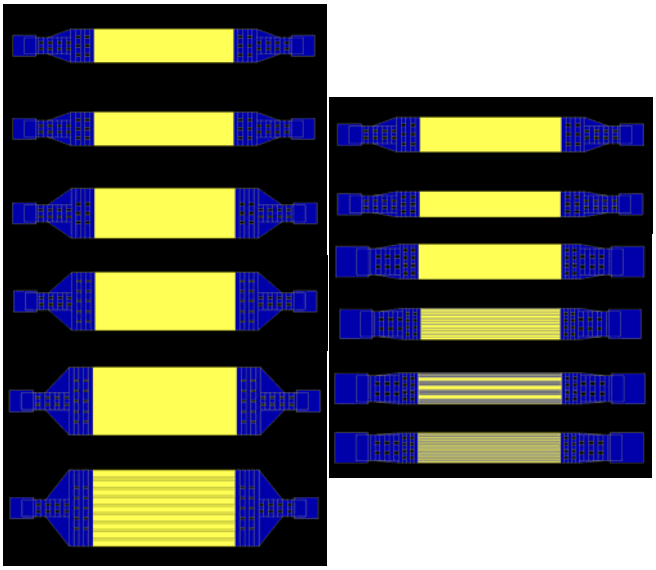

Fig. 7. Schematic of the transparency mask designs

(a) (b) (c)

Fig. 6. Photographs showing $Ni_{80}Fe_{20}$ multi-core structures with the following dimensions:

	Structure (a)	**Structure (b)**	**Structure (c)**
Strip thickness / nm	200	200	200
Overall sensor length (including bondpads) / μm:	65 060	65 000	65 000
Overall sensor width / μm:	7980	7980	9970
Metal line length / μm:	30 000	30 000	30 000
Metal width / μm:	60	20	20
Spacing / μm:	20	20	30
Total number of stripes:	100	200	200

The sensitivity measurements on the obtained structures revealed that the sensitivities of obtained structures were generally low. The actual value of the sensitivities cannot be quantified as the field generated in the laboratory could not be too large. This low value of the sensitivities was attributed to the quality of the sputtered $Ni_{80}Fe_{20}$ material. The sputtering base pressure of the sputtering machine was rather high and as such, oxidation and contamination readily occurred during the sputtering process, giving rise to lower permeability of the sputtered magnetic materials. It should be mentioned that currently the sputtering work is repeated using another sputtering machine with lower sputtering pressure, and the sensitivity measurements will be carried out on the sputtered materials. However, due to the time constraint (by the dateline of this project), the results could be included in this report.

4. Design, development and characterization of a microscale wire structured Insulator/ $Ni_{80}Fe_{20}$/Insulator material

4.1 Methodology

The main approach used was template assisted electrodeposition. Since the template fabrication was done by laser drilling and the laser beam available in this project was at micro scale rather than nanoscale, micro wire structure insulator/$Ni_{80}Fe_{20}$/insulator material was produced by template electrodeposition, in the following steps:

(a) A copper substrate was machined to dimensions of 1.5 cm x 2.5 cm x 0.3 cm.

(b) *Nano-turning* – the copper surface undergoes nano-turning, achieving a mirror-like finish. This helps to ensure that the specimen is in excellent condition for the electrodeposition process. This stage of the fabrication process is necessary as the condition of the substrate greatly affects the properties of deposited material layer. Before the template material is applied on the copper substrate, the substrate is dipped in diluted hydrochloric acid followed by distilled water. This is to remove any oxide layer formed on the copper substrate (Fig. 9(a)).

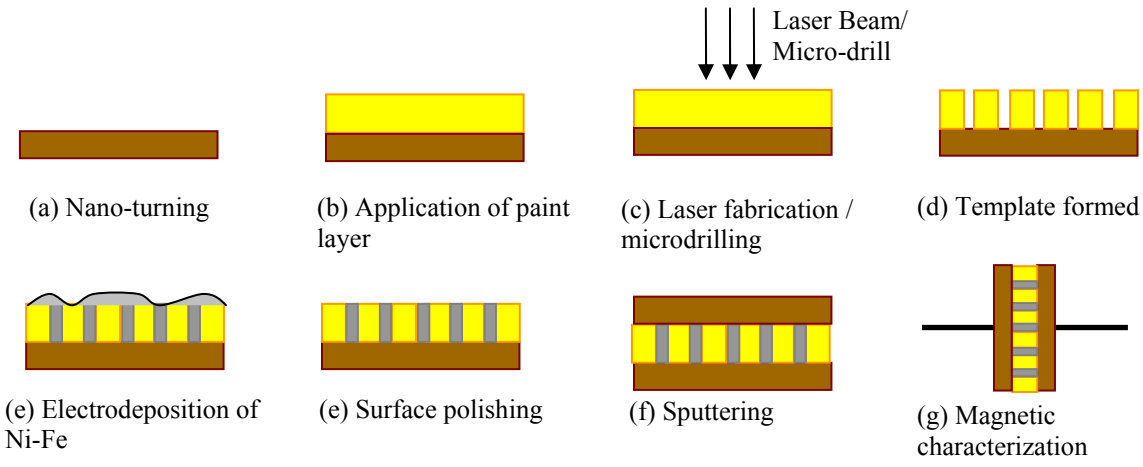

Fig. 9. Summary of fabrication process for multi-core sensing element by template electrodeposition.

(c) *Application of paint layer* – paint was applied layer by layer onto the mirror-like copper surface and soft-baked in between to achieve the required height. It should be

noted that the thickness of the paint at the centre was lesser than that at the sides (Fig. 9(b)).

(d) *Laser fabrication/ microdrilling* – an array of holes was machined on the paint layer, preferably at the centre of the paint layer where the surface tends to be more uniform. This is achieved either by laser fabrication technique or by micro machining technique. Hence, the template for electrodeposition had been obtained (Fig. 9(c)).

(e) *Electrodeposition of Ni-Fe* – an essential stage that was to be carried out prior to template electrodeposition is to cleanse the copper substrate surface to remove any copper oxide layer. This was done through acid dipping and thereafter rinsing the substrate in distilled water. After electrodeposition has been carried out, the paint layer can be removed to allow for characterization of the deposited structures (Fig. 9(d)).

(f) *Surface polishing* – the copper substrate underwent surface polishing before a thin layer of copper was sputtered onto it. This is to ensure that the specimen has a uniformly flat top surface that would facilitate the sputtering process (Fig. 9(e)).

(g) *Sputtering* – a thin layer of copper (approximately a few microns thick) is sputtered onto the template material so that magnetic characterization of the deposited structures can be carried out (Fig. 9(f)).

(h) *Magnetic characterization* – it involved characterization of the magnetic properties of the deposited structures in terms of sensitivity and coercivity (Fig. 9(g)).

4.2 Results and Discussion

4.2.1 Electrodeposition of Hollow and Solid Micro-Pillars by the Manipulation of the Substrate Surface Profile

Electrodeposition of Ni-Fe onto a copper substrate surface covered by a patterned template was carried out by means of DC electrodeposition using a DC power supply (Advantest R6243) as the external power source. The electrolyte solution was prepared by mixing boric Acid (H_3BO_3), nickel chloride ($NiCl_2.6H_2O$), nickel sulphate ($NiSO_4.6H_2O$), iron sulphate ($FeSO_4.6H_2O$) and saccharin. The electrolyte solution was

maintained at a temperature of 55°C and a pH of 3.4. The electrodeposition setup consists of an acrylic solution tank with air bubbles inlets, an air pump for introducing bubbling condition during electrodeposition process, a cathode rocker that allows the specimen to move back and forth in the electrolyte solution, a cathode rocker speed controller, a quartz coated cartridge heater, Teflon coated thermocouple temperature sensor, a digital temperature controller and a stainless steel plating cell that acts as an anode.

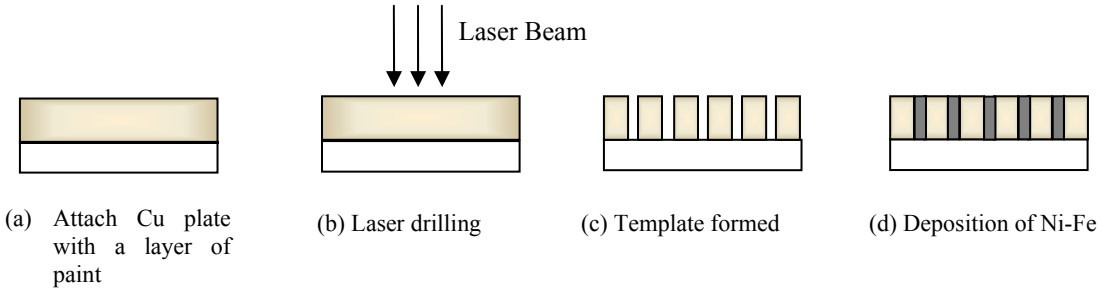

Fig. 10. An outline of the process sequence to fabricate Ni-Fe micro-pillars arrays using laser micro-machining and electrodeposition.

The template preparation was started by applying a layer of paint on top of a nano-polished Cu substrate, which was prepared using nano-turning machining technique. The paint was used in this process due to its low melting point. The paint layer was then soft-baked at 150ºC for 90 minutes in order to evaporate the paint solvent and to make the paint layer denser. Lastly, arrays of micro-holes were drilled on the painted layer by using laser micro-machining technique. Fig. 10 outlines the process sequence of the fabrication of Ni-Fe micro-pillars arrays. The surface and height of the deposited Ni-Fe pillars were observed using scanning electron microscopy (SEM).

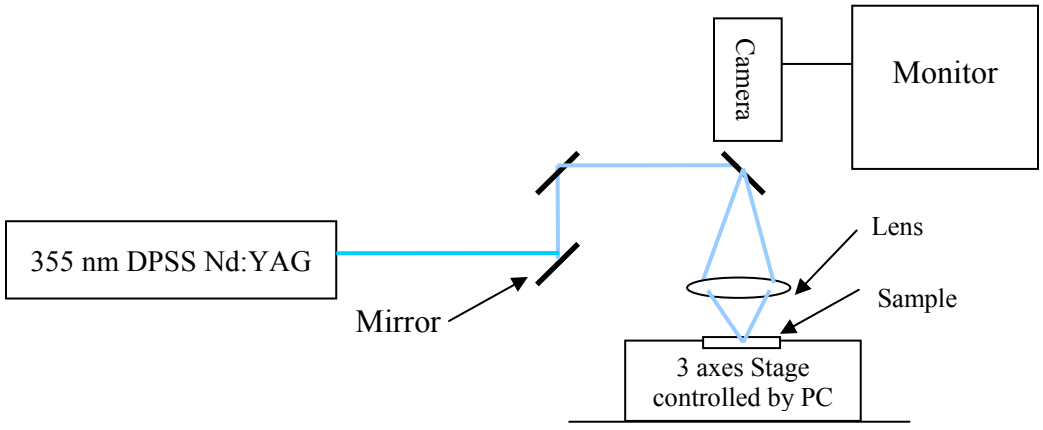

Fig. 11. Experimental setup of template fabrication process by laser.

The schematic diagram of the experimental setup of the laser fabrication for the template electrodeposition is shown in Fig. 11. The laser employed in this work was carried out by Coherent AVIA 3rd harmonic DPSS Nd:YAG laser with TEM_{00} (355nm, 30ns). The laser fluency was controlled by the variations of the employed parameters. The samples are copper substrates with coats of paint of varying thicknesses.

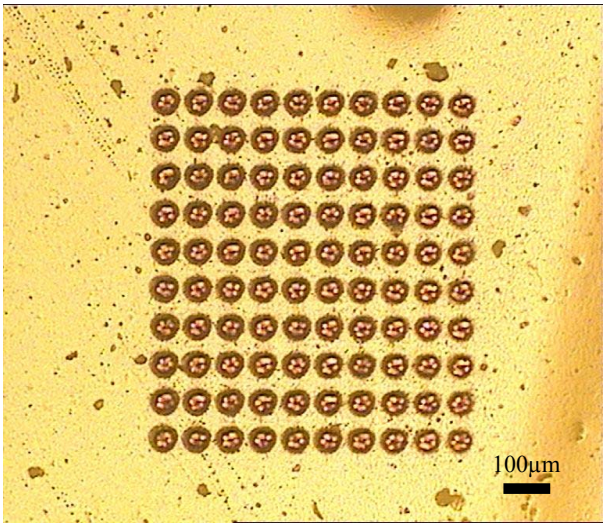

Fig. 12. A 10 x 10 array with an average spot size of 33.68 µm and an average pitch between adjacent spots of 70 µm.

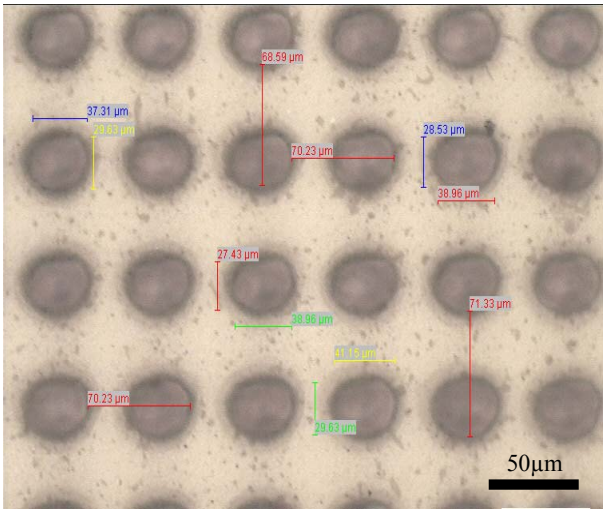

Fig. 13. Measurements of average laser spot size and average pitch.

A sample was placed onto the 3 axes stage, which was controllable by a computer. A suitable site for the array formation was selected and focused with a plano-convex lens. A CCD camera connected to a monitor was set up which enabled the entire laser drilling process to be viewed in real time. An algorithm for the array formation was designed for the stage to move in precise and calculated steps. A 10 x 10 array was fabricated as shown in Fig. 12. Fig. 13 shows the measurements obtained for the calculation of the average laser spot size and average pitch of 70 μm between 2 adjacent laser spots. The optimized set of parameters employed in the fabrication of this 10 x 10 array utilized a pulse mode, with a repetition rate of 4500 Hz, exposed for 300 milliseconds with a single laser pass. This will result in an average laser spot size of 33.68 μm, corresponding to a laser fluency of 0.75 J/cm^2.

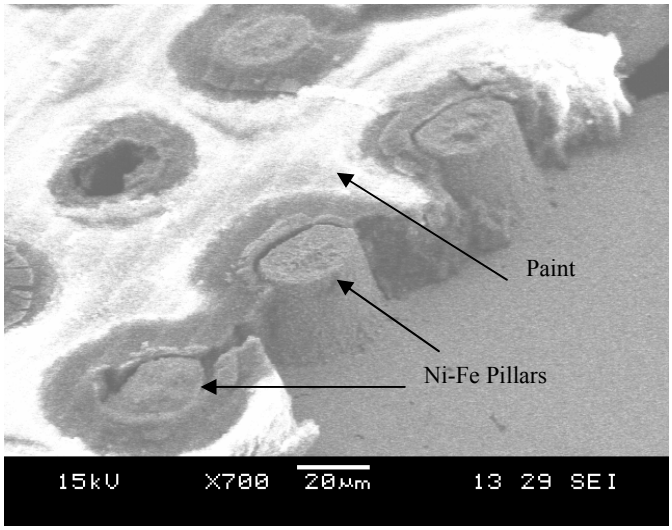

Fig. 14. SEM micrographs of the deposited Ni-Fe pillars of ~20 μm in height with smooth wall surface.

Fig. 14 shows that the Ni-Fe was successfully infiltrated into the template with 100 micro-holes of 20 μm depth. After the removal of the painted layer, it was observed that deposited Ni-Fe pillars were found to be 20 μm as defined by the thickness of the paint layer. In addition, the wall surfaces of the pillars were found to be very smooth. The surface morphology of pillars should be heavily dependent on the inner wall profile of the

micro-holes and the smooth surfaces of the Ni-Fe pillars showed that the surface morphology of the inner hole of the paint layer was also smooth. This result demonstrated that electrodeposition is a promising 'bottom-up' deposition method to allow complete infilling for high micro-pillars.

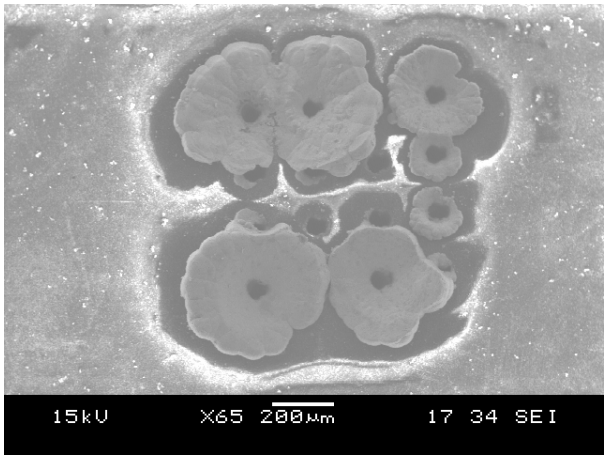

Fig. 15. SEM micrographs (top view) of the deposited hollow Ni-Fe tubes in 16 micro-holes.

Rather than growing Ni-Fe solid pillars by electrodeposition on flat copper substrate surfaces, it was interesting to see the formation of Ni-Fe hollow pillars on the drilled concaved copper substrate surfaces by electrodeposition, as shown in Fig. 15, in which the electrodeposition process duration was deliberately increased to ensure that the Ni-Fe deposited would grow out of the template holes, with a hole in each of the Ni-Fe pillar.

Interestingly, it was observed that the Ni-Fe was over-deposited, had grown out from the template holes and formed hollow Ni-Fe pillars or tubes (see Fig. 16(a)) instead of solid pillars. The formation of hollow Ni-Fe pillars after electrodeposition is believed to relate to the surface profile of the copper substrate. During the laser machining process on the painted layer, micro-holes were formed within the copper substrate itself in this case. As shown in Fig. 16(b), the deep micro-hole profile of the copper substrate surface could result in a tendency for the Ni-Fe to be deposited on the circumferential regions of the micro-holes, which are all conductive, thus forming hollow Ni-Fe tubes. The hollow pillar deposition mechanism makes it possible to develop multi-layer composite micro pillars through template electrodeposition. For example, in order to make Ni-Fe/Cu composite micro pillars, the copper substrate surface for each of the template holes will be made concaved, Ni-Fe will firstly be deposited to form hollow pillars, and then the second run of deposition will be made by depositing copper to form copper core of each of the Ni-Fe pillars. Multiple layer pillars can be deposited in a similar method.

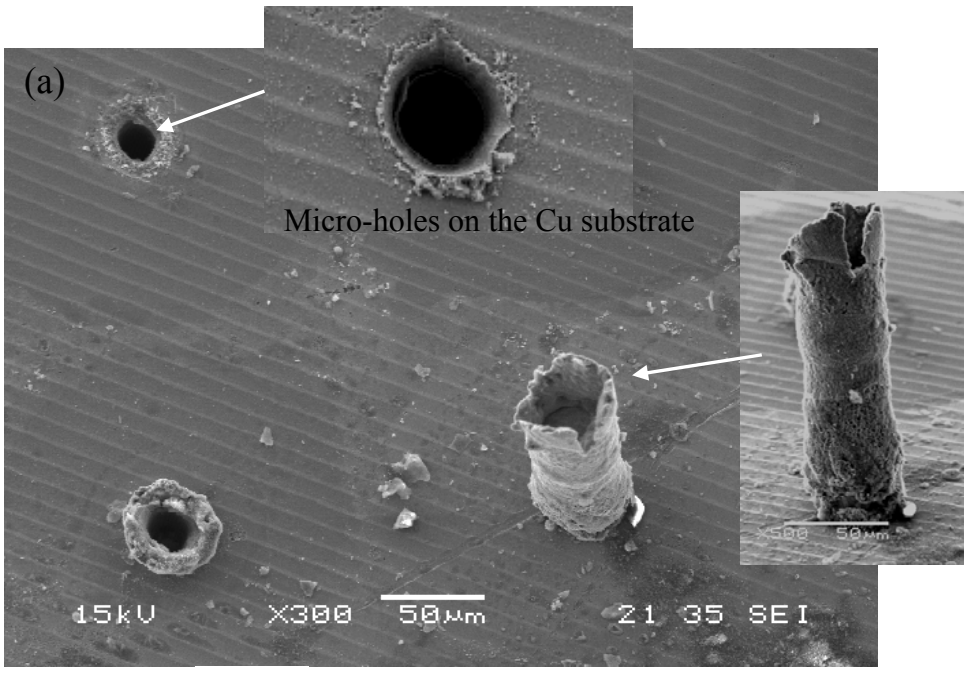

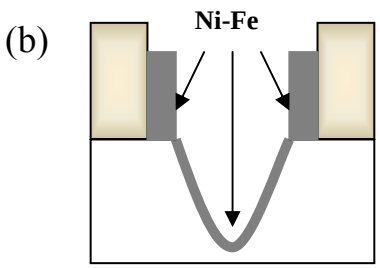

Ni-Fe tends to deposit preferentially on the circumferential region of the micro-holes

Fig. 16. (a) SEM micrograph showing the deposited Ni-Fe hollow tubes after removal of the painted layer on the copper substrate and the concaved or holed surfaces of the copper substrate made by laser machining process; (b) schematic illustration of the formation of hollow Ni-Fe micro-tubes on concaved or holed copper substrate by electrodeposition.

In conclusion, micro Ni-Fe pillars of high aspect ratios were successfully grown on Cu substrates by template-assisted electrodeposition. The template was made of paint on copper substrate, having multiple holes produced by laser drilling. One of the benefits of using the laser fabrication technique is the capability to prepare different kind of surfaces of the copper substrates, such as flat or concave substrate surfaces. When template electrodeposition was carried out on flat substrate surfaces, solid Ni-Fe pillars were grown, whereas when the deposition was carried out on concave substrate surfaces, hollow Ni-Fe pillars were grown. This phenomenon could be useful to fabricate hollow Ni-Fe pillars for better sensing performance.

4.2.2 Comparison of Quality of Templates Fabricated by Mechanical drilling and by Laser Fabrication Technique

Two fabrication methods for the holes on template were used in this project: 1) mechanical drilling, and 2) laser drilling, including making the hole profiles, surface profiles of the copper substrate and the deposited structures.

As observed in Fig. 17(a), for template fabrication using mechanical drilling, the hole profile obtained tend to be circular, while the hole profile of template fabricated using laser drilling tend to be non-circular due to the associated heat affected zones in the laser process (Fig. 17(b)). This can be attributed to the spherical aberration and non-circularity of the laser beam.

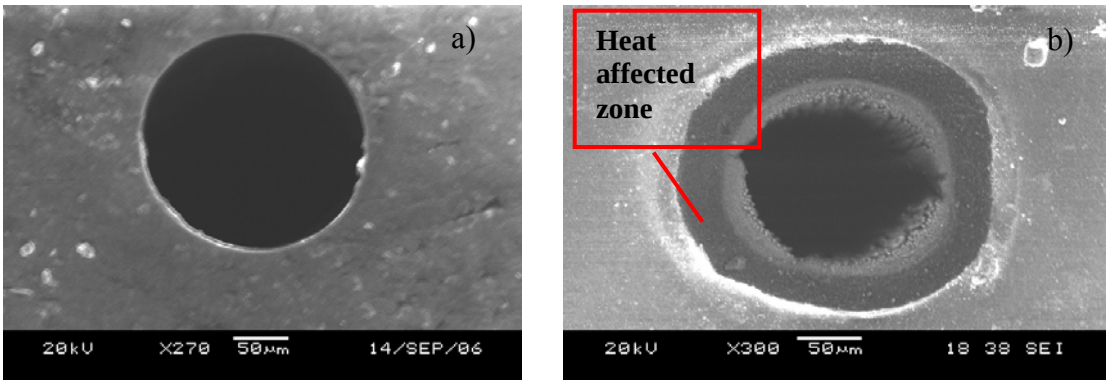

Fig. 17. SEM photos showing (a) circular hole profile by mechanical drilling; (b) non-circular hole profile (with heat affected zones) by laser drilling.

It was noted that although the mechanical drilling technique is capable of producing better hole quality, the current technology can only achieve the minimum hole diameter of about 100 µm, whereas laser fabrication technique can make the hole diameter down to 20 µm, despite the associated tapering effect. Further to mechanical drilling, as the drill bit has a tapered tip, tapered indentation was made on each of the copper substrate (Fig. 18(a)). In the process of electrodeposition, the material tends to deposit along the circumference of the base of the fabricated holes. Hence, there is a high possibility that hollow pillars are formed in the template electrodeposition, as shown in Fig. 18(d). In the case of laser fabrication technique, the indentation on the copper substrate can be flat or concave, as seen in Fig. 18 (b) and (c), respectively. During template electrodeposition, solid pillars grown on flat copper substrate (Fig. 18(e)), whereas hollow pillars grown on concave copper substrate (Fig. 18(f)).

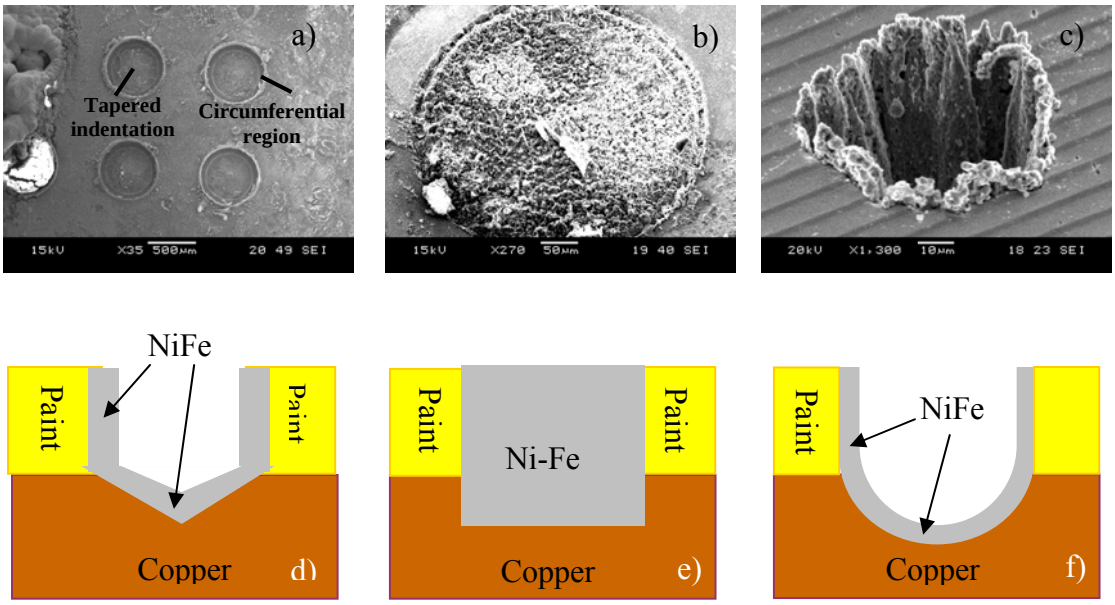

Fig. 18. SEM images: (a) tapered indentations on the Cu substrate by mechanical drilling, (b) flat indentations on the Cu substrate by low laser fluence drilling, and (c) round/concave indentations on the Cu substrate by high laser fluence drilling; schematic diagrams: (d) deposited hollow micro wires from mechanically drilled substrates, (e) solid micro wires resulting from the formation of flat indentations from low laser fluence drilling, (f) hollow micro wires resulted from the formation of round/concave indentations.

It was be noted that using different laser systems could have different results. Holes fabricated using UV laser had better surface profiles as compared to those fabricated using green laser. The thermal damages done to the non-machined regions using UV laser machining was minimized as reflected in the minimal heat affected zones (Fig. 19(a)). On the other hand, specimens machined using green laser had very rough top profile (Fig. 19(b)). There was a significant increase in the heat affected zone for the machined holes as compared to those obtained using UV laser.

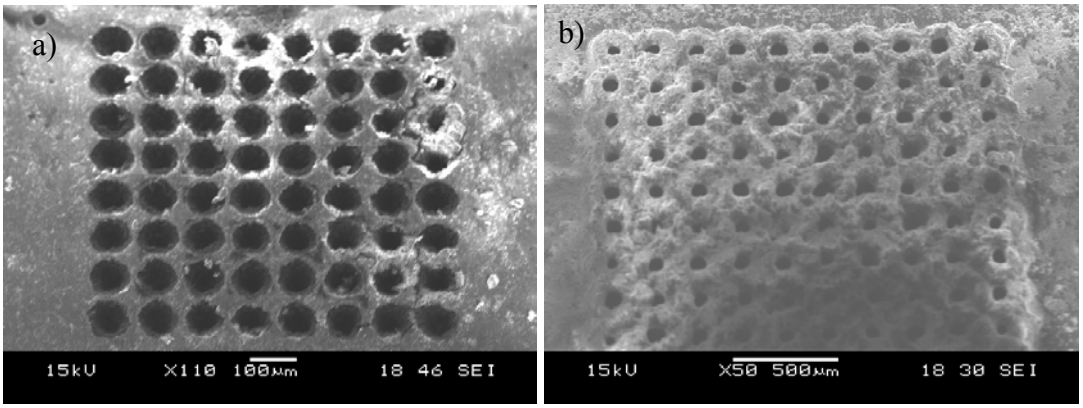

Fig. 19. (a) Template fabricated using UV laser; (b) template fabricated using Green laser.

Laser machining is one of the high precision fabrication techniques to obtaining micro arrays. It is normally used to machine holes of smaller diameter. This is a major advantage of this method as arrays of smaller dimensions can be achieved. Further, this method is fast and allows for high accuracy. As laser machining is programmable, it allows for high repetition rate.

4.2.3. Structure of Electrodeposited Ni-Fe

In this study, XRD measurement was performed on a thin film of Ni-Fe to check the metallic crystal structure, as well as the average crystalline size of the deposited material. Electrodeposition of the thin film was carried out at a current density of 45 A/dm^2 and a plating time of 1 hour. Fig. 20 shows the XRD graph of counts per second against 2θ angle obtained from XRD. Five obvious peaks were observed at the following 2θ angle values of 44.28°, 51.53°, 75.87°, 92.20°, and 97.70°, and their corresponding Miller indices are obtained. Using the 2θ angles, the following calculations are shown in Table 1.

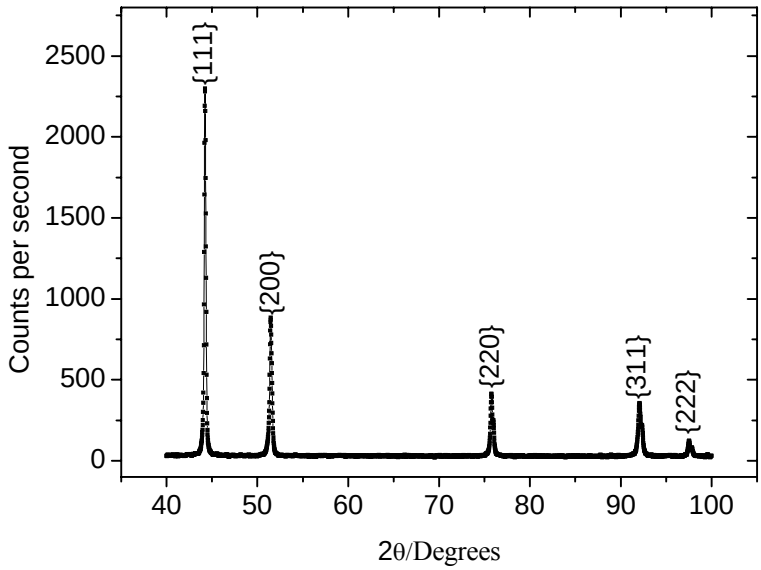

Fig. 20. Graph of counts per second against 2θ angle

Table 1. Calculations from XRD results.

2θ (deg)	**θ (deg)**	**sin θ**	**$\sin^2\theta$**	**{hkl}**	**$h^2+k^2+l^2$**
44.28	22.14	0.377	0.142	111	3
51.53	25.77	0.435	0.189	200	4
75.87	37.94	0.615	0.378	220	8
92.20	46.10	0.721	0.520	311	11
97.70	48.85	0.753	0.567	222	12

Since $\sin^2 22.14 / \sin^2 25.77 = 0.142 / 0.189 \approx 0.75$, the crystal should have face-centered cubic (FCC) structure.

The lattice constant, a = $\lambda \sqrt{(h^2 + k^2 + l^2)} / 2\sin\theta$

= $(0.154 \sqrt{3}) / (2 \times 0.377)$

= 0.354 nm

It was thus identified that the metal tested was Ni-Fe, with a FCC structure and a lattice constant of 0.354nm.

The peak positions of the Ni-Fe thin film was compared with that of the standard Ni-Fe in the database. Besides scanning the specimen, a standard silicon sample (Si 070226) was also scanned and compared to the standard Si standard peak positions, so as to remove systematic errors in the calculations of the average grain size. The calculations of the grain size (in Å) were carried out using a software (Pmgr MFC Application, version 1.0.0.1). The results are as shown in Fig. 21.

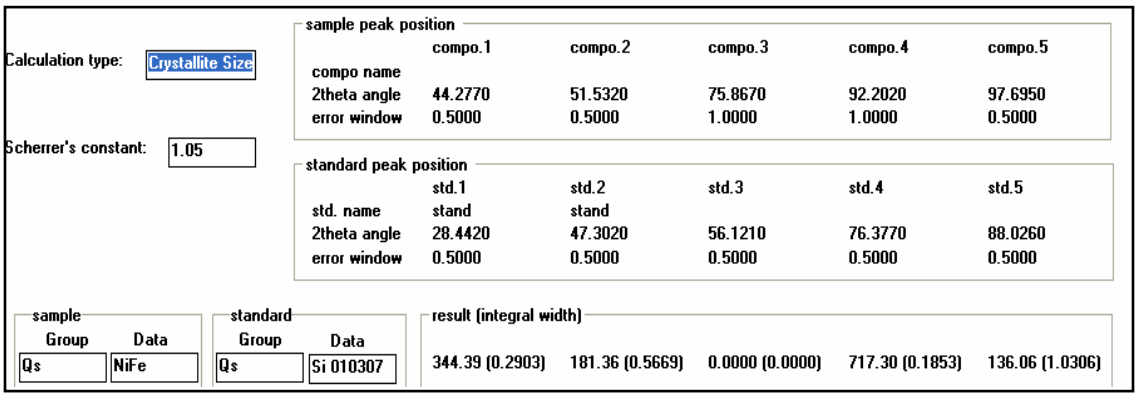

Fig. 21. Results of calculations for the grain size using the software.

Table 2. Summary of the grain size results (1 angstrom = 1.0×10^{-10} m = 0.1 nm)

	Grain size (in Å)	Grain size (in nm)
	344.39	34.439
	181.36	18.136
	717.3	71.73
	136.06	13.606
Average	344.78	34.48

The grain size was taken as the average of the four values of the grain size calculated, which is 34.48 nm.

4.2.4. Fabrication of Sensing Element Arrays using Template Assisted Electrodeposition

In order to test the difference in sensitivity when the array size is changed, a special template having four arrays was fabricated. The template has four spots, containing 16,

36, 64 and 100 holes, respectively (Fig. 22). The electrodeposited sample using the template allows for measuring the sensor sensitivity varying against variation of the number of cores in the sensing element.

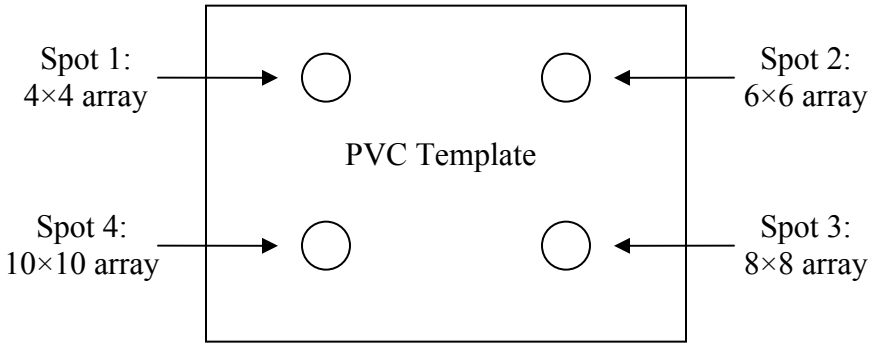

Fig. 22. Schematic diagram of the arrangement of arrays on the template.

The template was pasted onto the copper before it was drilled, resulting in an ablated copper substrate surface. Again the average diameters of the holes were about 40μm. The electrodeposition parameters were all the same as before. The value of the current density was 7368A/dm^2. It should be mentioned again that this is a theoretical value as the actual value was changed by various factors mentioned in the above section. The whole process took 5 hours 20 minutes. All the four array of holes were deposited with Ni-Fe (Fig. 23).

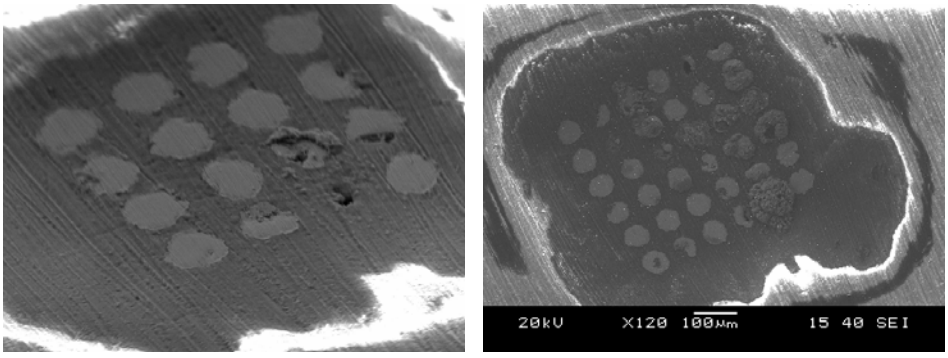

(a) (b)

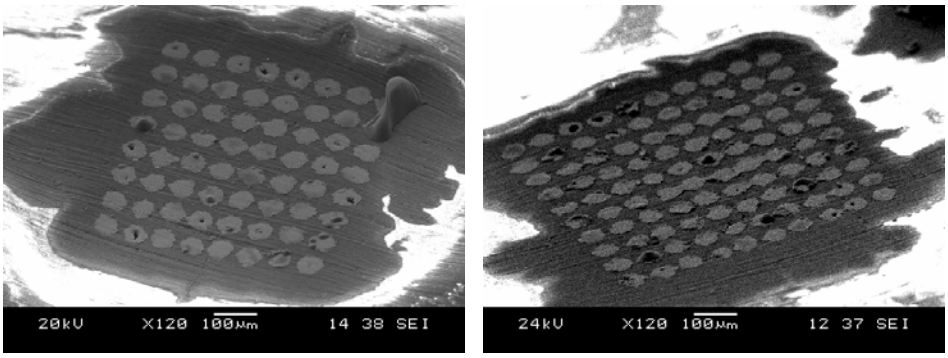

(c) (d)

Fig. 23. SEM pictures of the various arrays after electrodeposition: (a) 4×4 array; (b) 6×6 array; (c) 8×8 array; (d) 10×10 array.

A layer of copper was then sputtered onto the arrays of electrodeposited $Ni_{80}Fe_{20}$ wires as a connector, so that the testing current can be imposed onto the $Ni_{80}Fe_{20}$ wires, as shown in Fig. 24. However, due to the insufficient length of the deposited multi-cores, the sensitivity of the sensing unit was very low.

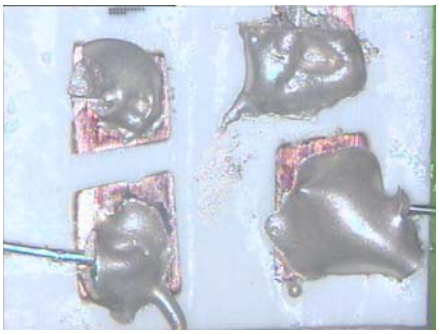

Fig. 24. Top view of soldered arrays of multi-core arrays sensing elements (1mm thick)

It was intended to test the sensitivity of the sensor in variation with the 4 different arrays of sensing element. In order to place the arrays of $Ni_{80}Fe_{20}$ pillars at the centre of the pickup coil (27 mm in diameter) and in the correct orientation, the substrate has to be cut to the appropriate size. The dimension of the substrate on which $Ni_{80}Fe_{20}$ pillars were deposited was 50 mm (length) by 15mm (width) by 3mm (thickness). A laser machine

was used for cutting the substrate. However, the cutting could not be done unsuccessfully as the substrate absorbed excessive energy during cutting. As the consequence, the sensitivity test on the specimens could not be carried out.

5. Comparison between the magnetic properties of the stripe and wire structured composites

Due to the limitation of the sputtering machine used, the stripe composite samples made were too low in the magnetic permeability, as described in Section 2.1.2 (the sputtering base pressure of the available machine used was rather high and as such, oxidation and contamination readily occurred during the sputtering process, giving rise to lower permeability of the sputtered magnetic materials). Therefore, the magnetic properties of the stripe structure could not be concluded. Consequently, comparison between the magnetic properties of the stripe and wire structured composites could not be carried out. However, currently the sputtering work is repeated using another sputtering machine with much lower sputtering pressure, and the sensitivity measurements will be carried out on the sputtered stripe structured composite. A comparison of the magnetic properties between the stripe and wire structured composites will be made then.
At the mean time proper equipment will be found for cutting the substrate and the sensitivity test on the arrays of $Ni_{80}Fe_{20}$ pillars and stripes will be carried out.

6. Design, development and characterization of a wire structured Insulator/$Ni_{80}Fe_{20}$/Cu/ $Ni_{80}Fe_{20}$/Insulator material

6.1 Methodology

In order to develop and optimize a sensing element unit consisting of multiple composite wires in a specific arrangement as well as at a particular distance from each other, a method consisting of several stages of execution was proposed and adopted (Fig. 25).

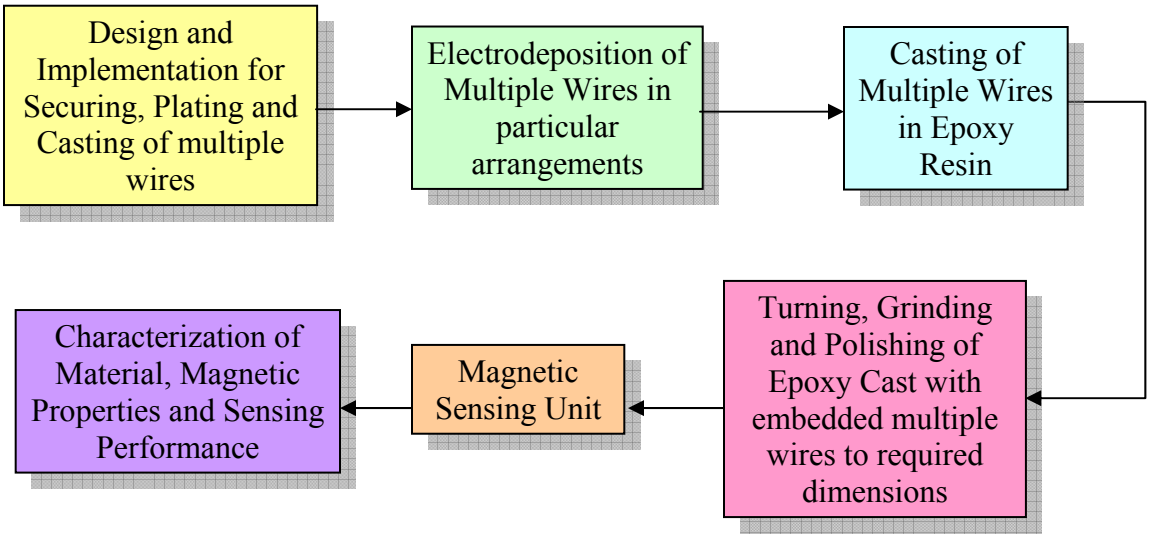

Fig. 25. Flow chart of the proposed project methodology, showing the various stages required to develop a sensing element unit.

A fixture has to be designed, tested and implemented to ensure the efficient securing of the multiple wires which is capable of holding copper wires in several arrangements during the electrodeposition and casting process. Multiple wires will then have to be secured in the fixture and electrodeposited to obtain composite wires of the required composition and thickness. Investigations will be conducted to understand the electrochemistry with electroplating multiple wires and also to verify the consistency of the method. The multiple wires, which are in a particular arrangement, are then embedded in an epoxy resin and once this is fully cured, the hardened unit will then be reduced to appropriate dimensions through turning and grinding. Once this is achieved, characterization of the sensing unit will be carried out in relation to its material, magnetic properties and sensing performance. The number of wires as well as the distance between the wires should be further manipulated and optimized.

6.2 Results and Discussion

6.2.1 Fixture design and implementation

In order to carry out electrodeposition and casting of multiple wires, a fixture has to be designed to achieve the following aims:

1) The fixture must be able to hold the wires in place and avoid any displacement during the process or the transitions.
2) The fixture must have sufficient opening to ensure maximum exposure of the copper wire (cathode) to the anode during electrodeposition
3) The arrangement of the wires can be controlled.
4) The fixture structure must be firm, but at the same, can be easily dismantled to ensure easy removal of the final cast sample.

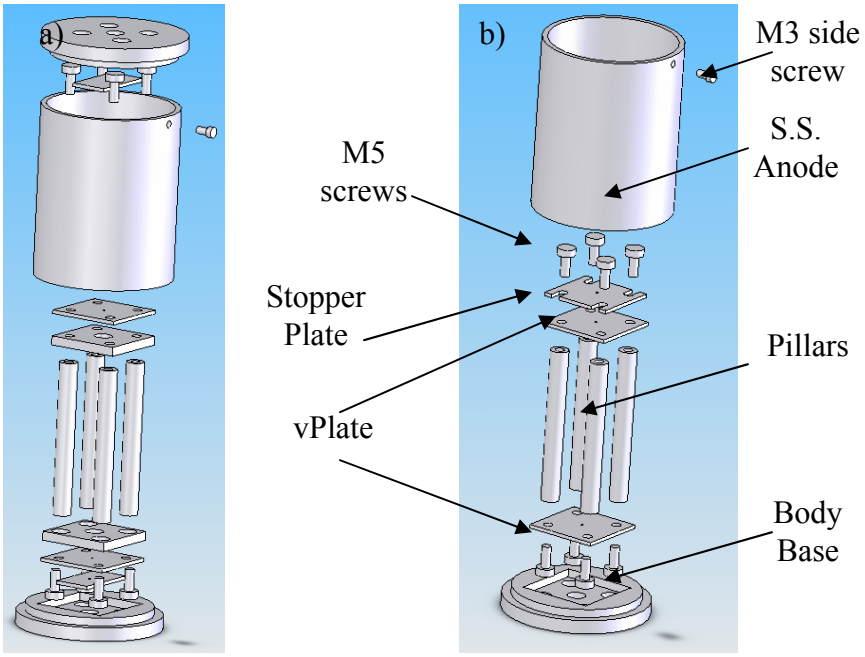

Fig. 26. 3-D drawings by SolidWorks on the (a) initial design; and (b) final designs.

Fig. 26 (a) shows the initial proposed design of the fixture. The initial design contains too many parts and makes assembly rather complicated, not efficient and does not ensure standard positioning of the multiple wires. Thus, a final design was proposed to counter such problems (Fig. 26(b)). The final design of the fixture basically involve several features: 1) stainless steel anode (for electrodeposition) and body base; 2) the main fixture structure, that holds the variable plates, containing the pillars, the screws and the stopper plate; 3) the top and bottom variable plates for ensure the location of the multiple wires. These plates will be changed according to the required distance between the wires.

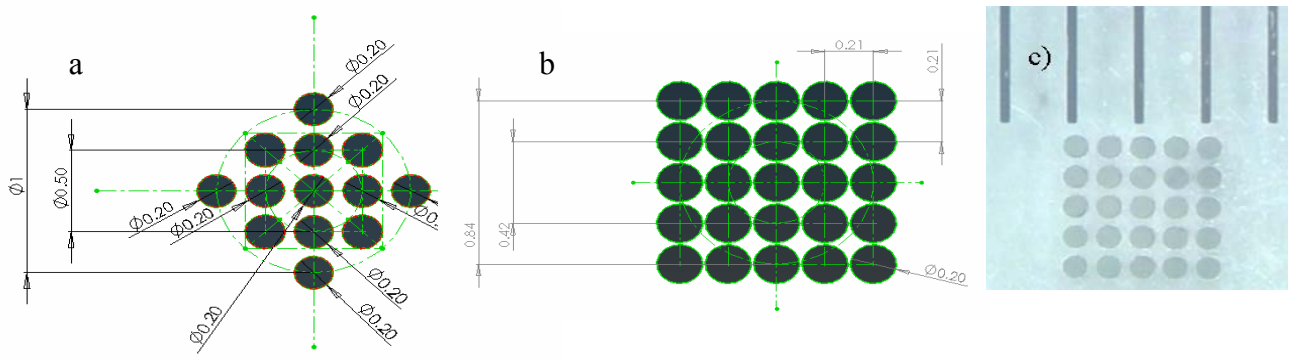

Fig. 27. Pictures showing the dimensions and arrangements of variable plates for (a) present design; (b) optimized design; (c) photo of fabricated holes with inter-black lines at scale 0.5mm.

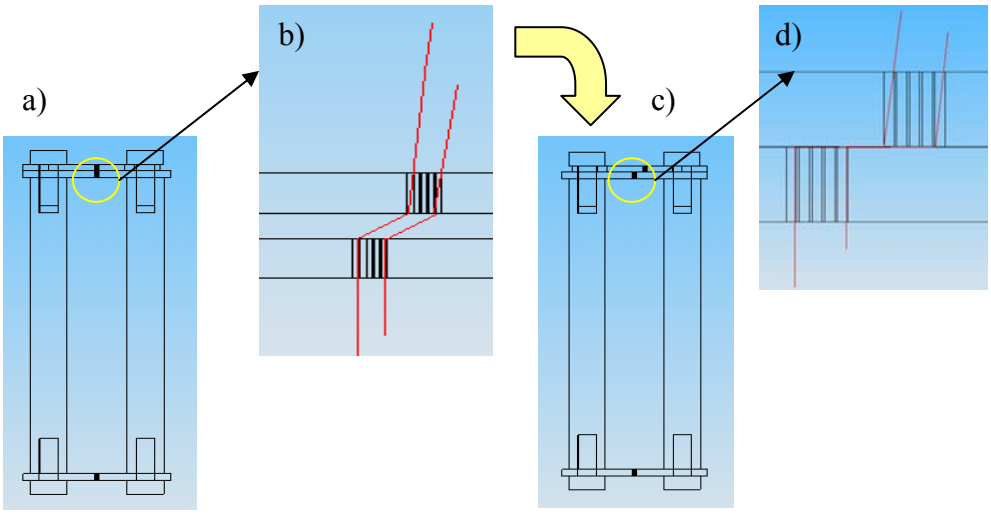

Fig. 28. Series of pictures showing the unique function of the stopper plate. (a) and (c) shows the position of the stopper plate before and after the securing of the wires into a standardized location, (b) and (d) shows the zoom-in of the earlier pictures.

Fig.27 shows the dimensions and arrangements of the top and bottom variable plates for the securing of the wires. Fig. 28(a) shows the present arrangements while Fig. 28(b) and (c) displays the intended and optimized design of the variable plates and the actual fabricated plate respectively.

Fig. 28 features the unique function of the stopper plate. With the presence of the stopper plate, the wires can be easily and firmly secured into their standardized location with relative ease. The entire design was then sent for fabrication and the assembled structure was presented in Fig. 29.

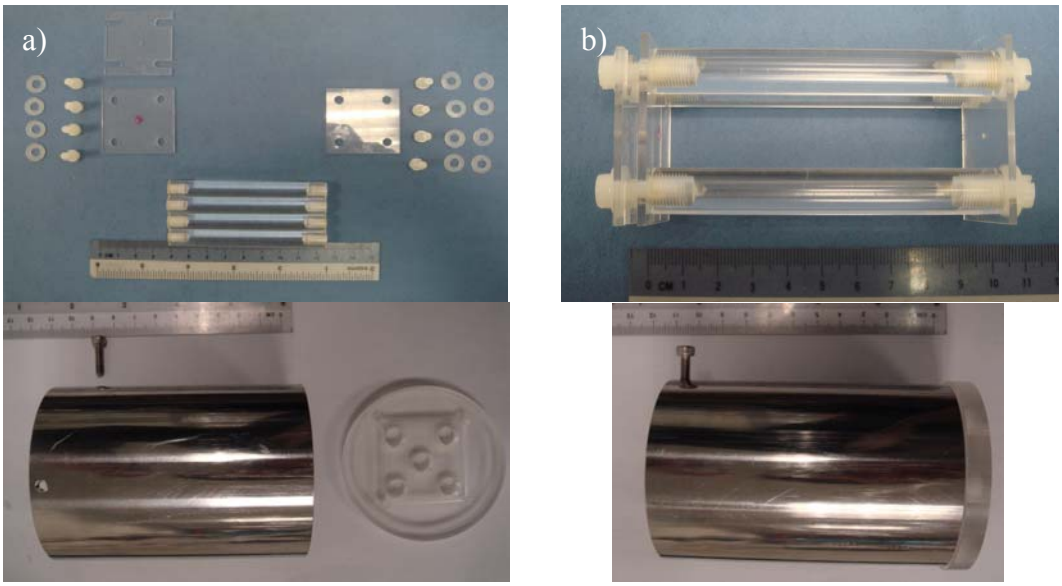

Fig.29. (a) Photos showing the entire range of the components of the design; (b) a close-up view of the assembled main body structure.

Fig. 30 shows the final designed fixture was tested and was found to be able to fix a various number of wires firmly at the standardized location throughout the entire length of the wires. This strongly indicates the success of the designed fixture in achieving the earlier listed aims.

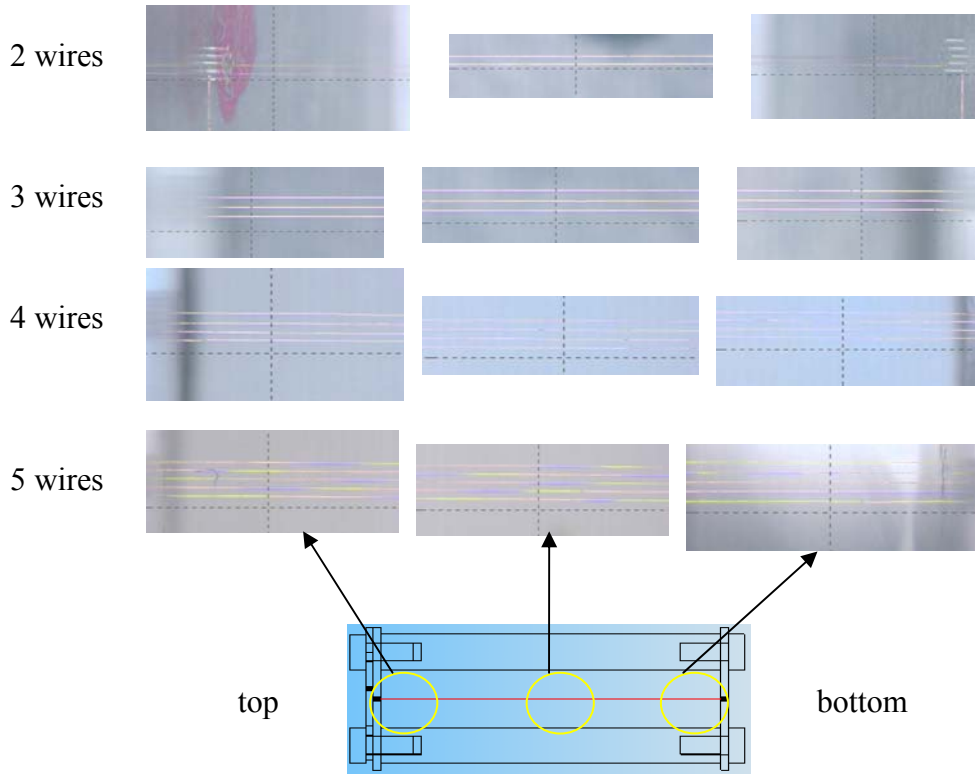

Fig. 30. Photos showing the maintained distance between the secured wires.

6.2.2 Effect of Number of Wires on Surface Profile, Fe%, Thickness and Current Efficency

Batches involving different arrays of 1, 3 and 5 wires were fabricated in order to study the effects of the number of wires on the resulting surface profile of the wires. Individual wire surface profile were observed and shown in the figures below.

Fig. 31 shows that there is generally no significant change in surface profile as the number of wires electrodeposited increases. Occasionally, the surface may look highly irregular. Upon examination, these are usually caused by residuals of Cl or S. Once in a while, pits may be observed randomly on the electrodeposited wires. But this is seldom observed in the current batch of samples.

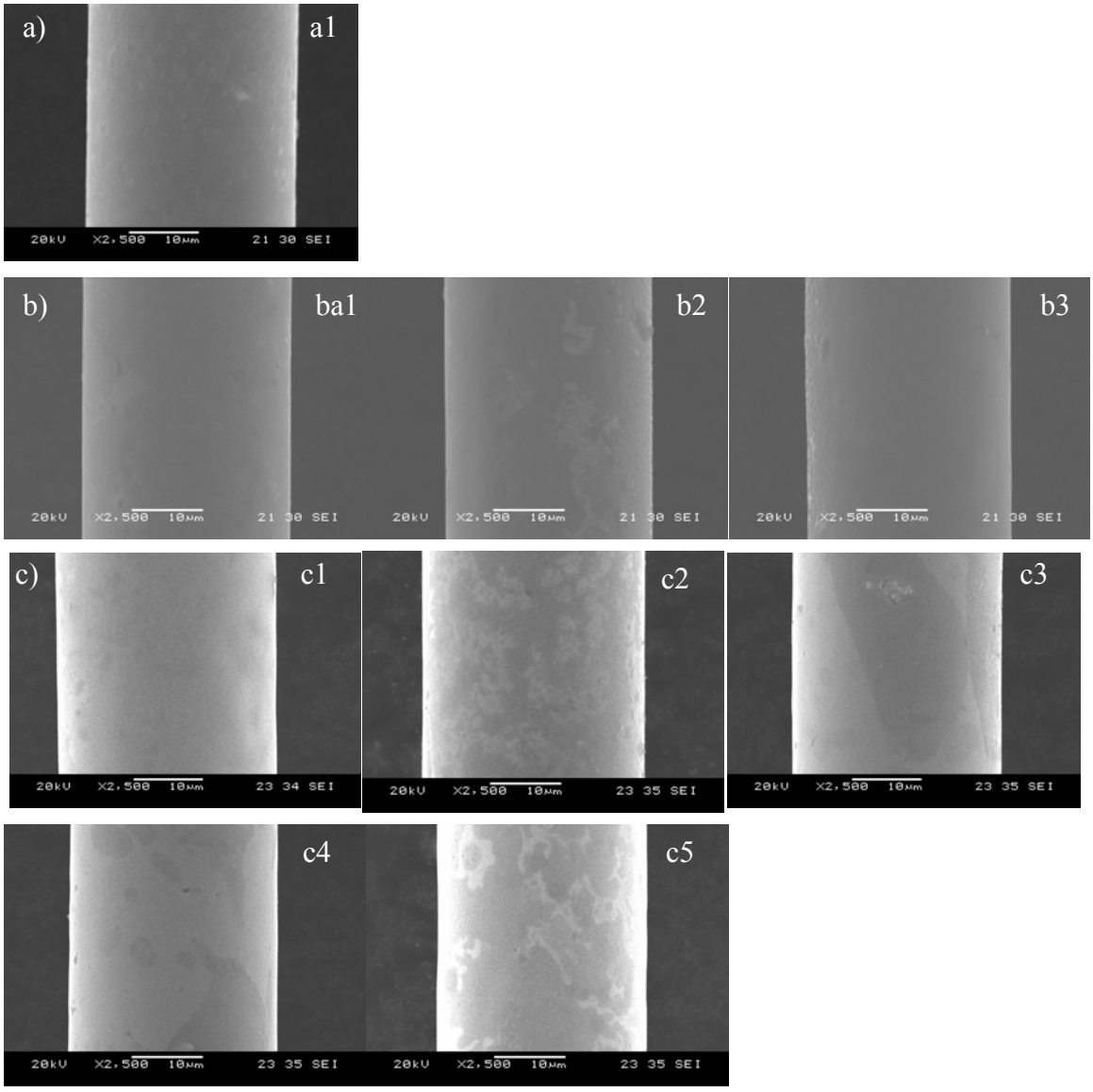

Fig. 31. SEM photos showing surface smoothness of electrodeposited wires Batch 1 with (a) 1 wire, (b) 3 wires, (c) 5 wires; in linear arrangements.

Fig. 32 shows the current batch of electrodeposited wires. The 2x2 array arrangement was not brought up since the earlier batch of electrodeposited wires only generated a 4 wire in linear arrangement sample. The surface profile of the current batch seems to be as smooth as that of the earlier batch as shown in Fig. 31.

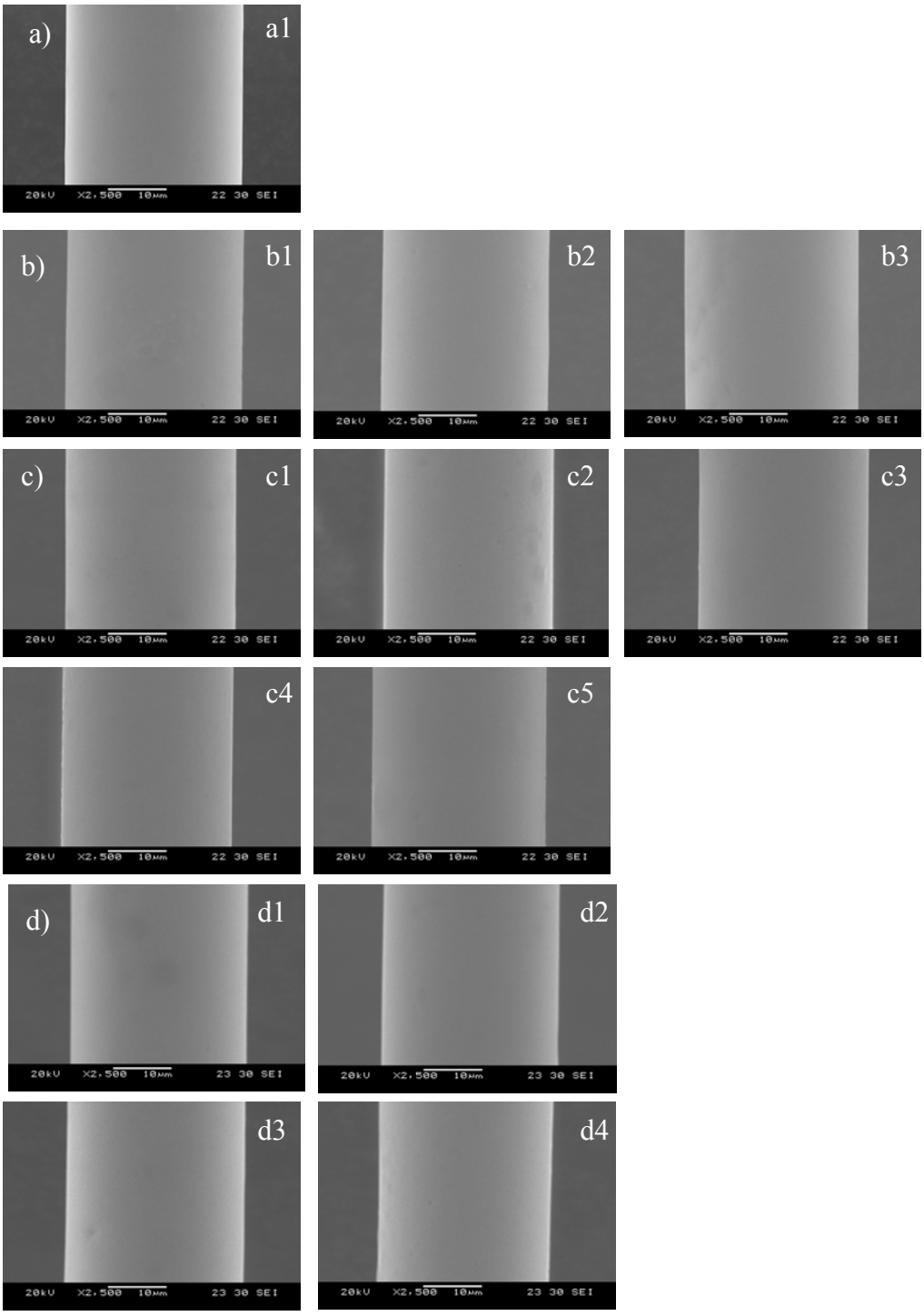

Fig. 32. SEM photos showing the surface smoothness of electrodeposited wires Batch 3 with (a) 1 wire, (b) 3 wires in linear arrangement, (c) 5 wires in linear arrangement, and (d) 2x2 wires in array arrangement.

This is expected to be the case since it is a repeat of the experiment whereby the pH, current density, plating time and temperature are all kept constant. However, the SEM photos for the current batch seem less clear as the previous batch of photos.

The effect of the number of wires on the resulting Fe% was investigated by measuring the composition of all the individual wires in various batches and arrays (to ensure consistency).

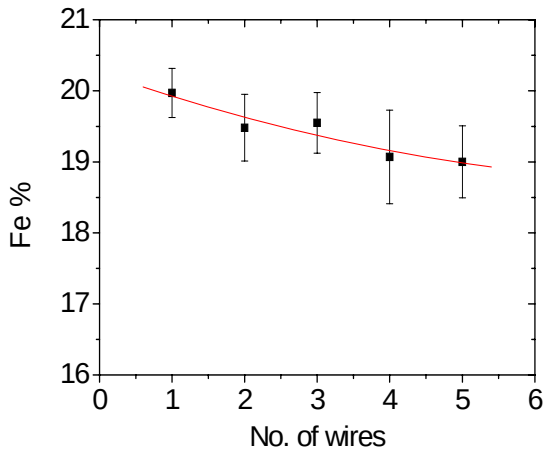

Fig. 33. Batch 1 graph of Fe% VS number of wires.

As the number of wires increases, the Fe% tends to decrease slightly from 20% to 19%. The 2x2 wires (4 wires) give a slightly higher Fe% because one of the three samples used to compute the Fe% is rather close to 20%. As the number of wires increases, the difference between the maximum and minimum value increases (as seen in the error bars). Upon examining each wire within in their respective arrangements, no observable pattern was found as to whether the inner or outer wires tend to have a higher or lower Fe%.

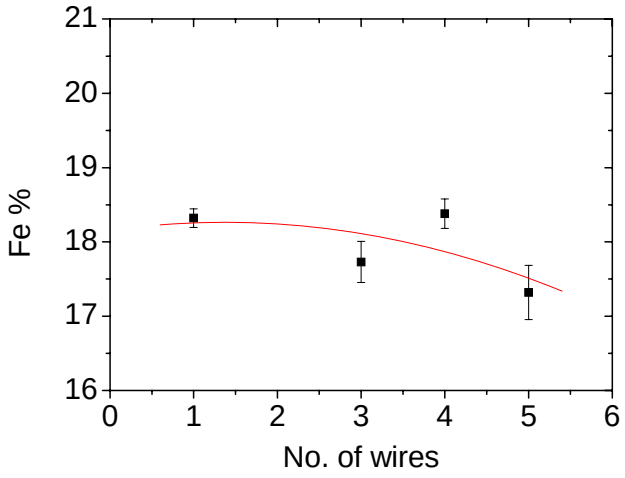

Fig. 34. Batch 3 graph of Fe% VS number of wires.

Fig. 33 and Fig. 34 show that both batches of electrodeposited wires generally show a downward trend to its Fe% as the number of wires increases. The decrease is likely to be caused by factors related to solution equilibrium and mass transportation of the ions within the diffusion layer. Since multiple wires are present, a region between the multiple wires may be lower in Fe% composition. This results in different solution equilibrium at the region. Furthermore, mass transportation of the ions is less efficient when more wires are present as these generate a wider region of solution non-equilibrium. The mild agitation provided by the higher plating temperature is generally not enough to replenish the loss of the Fe%. Thus, Fe% tends to decrease as the number of wires to be electrodeposited increases. This may also explain the trend of why electrodepositions at room temperature tend to yield a rather irregular Fe% along each individual length of the wire.

The effect of the number of wires on the deposited coating thickness for different batches was also investigated in this project and shown in Fig. 35 and Fig. 36.

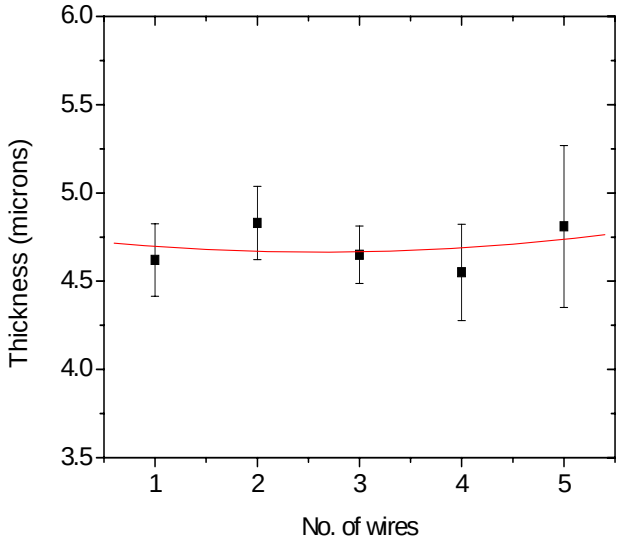

Fig. 35. Batch 1 graph of thickness (microns) VS number of wires.

Generally, there is no observable change in thickness as the number of wires increases. This indicates that current has passed through each of the wires properly and thus electrodeposition was rather consistent to each of the wires. Upon examining each wire in their respective arrangements, no observable pattern was found as to whether the inner or outer wires tend to have a higher or lower thickness. Fig. 28 and Fig. 29 show that both the wire batches show little changes in thickness as the number of wires increases. This is to be expected since the current density supplied to them is constant.

$$\text{Current density} = \frac{I}{A}$$

where I = current in A, A = area in dm^2

Since area changes as the copper core gets electrodeposited, the current density changes slightly with increasing thickness. However, as long as the current passing

through each wire is evenly distributed, current density should be similar in the course of electrodeposition. This may be an issue if certain part of the wire length has a dent or

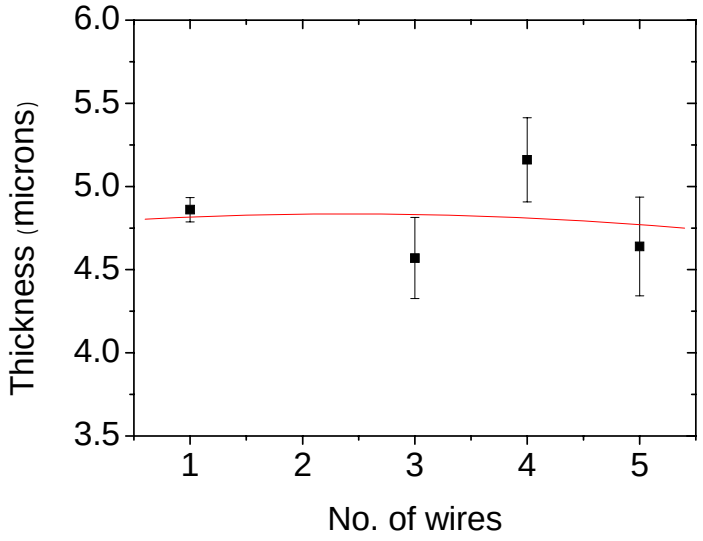

Fig. 36. Batch 3 graph of thickness (microns) VS number of wires.

depression. This causes the resistance at that point to be higher and some current may travel preferentially to another wire length. The result will be some wires being higher in thickness. Occasionally, this is encountered.

Fig. 37 shows that there is generally no change in current efficiency as the number of wires increases. As a result of its relation with the thickness, its maximum and minimum values as denoted by the error bars are similar to that Fig. 36. Fig. 37 and Fig. 38 shows that the two batches of wire samples show little changes in its current efficiency as the number of electrodeposited wires increases. The current efficiency was maintained at around 95%, which is considered high in nickel-iron plating baths. This indicates that only a small amount of current is being converted to energy to encourage the chemical reaction responsible for hydrogen evolution.

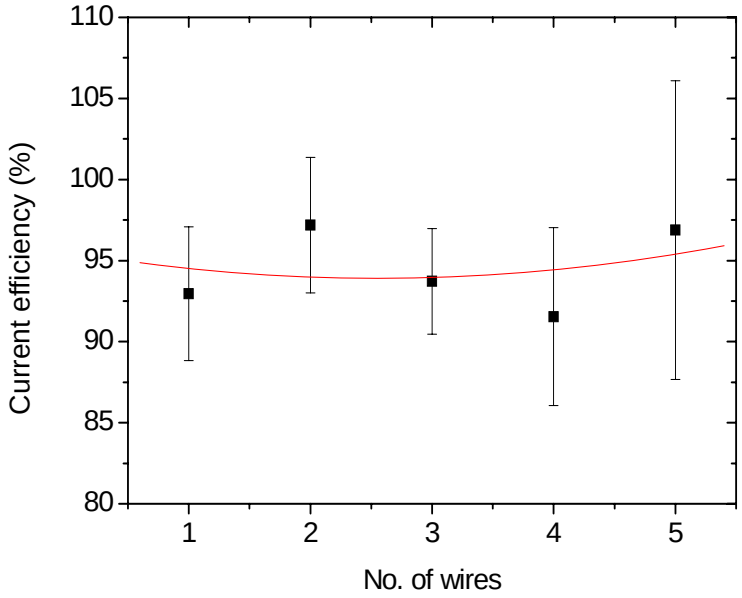

Fig. 37. Batch 1 graph of current efficiency (%) VS number of wires.

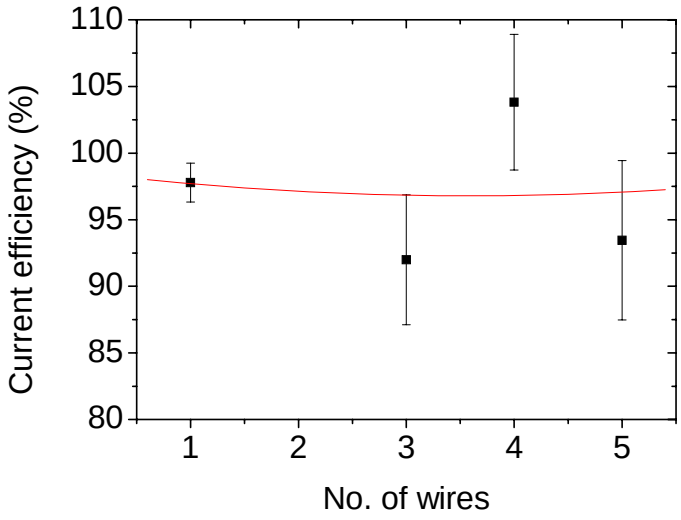

Fig 38. Batch 3 graph of current efficiency (%) VS number of wires.

6.2.3 Effect of Number of Wires & Arrangement on Magnetic Properties

In the study, the sensing units were placed in a pick-up coil of 800 turns and 12mm in outer diameter. Out of the 4 samples generated for MI, only 2 samples (1 wire and 2x2 wires) showed response to the sensitivity test. Thus, analysis made here is mainly based on these 2 samples.

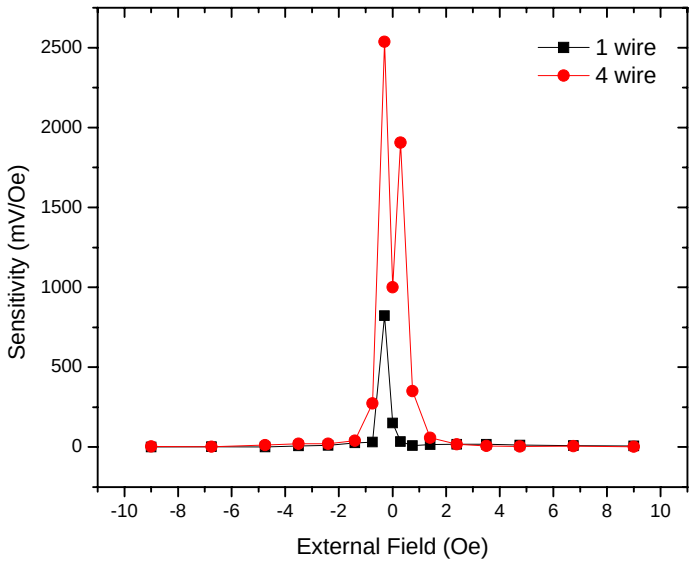

Fig. 39. Sensitivity plots for 1 wire and 4 wire arrangements.

The single wire sensing unit gives a sensitivity of around 850 mV/Oe (Fig. 39). In comparison, the 2x2 wires sensing unit gives a sensitivity of around 2500 mV/Oe. This is about factor 2.9 times. From this, the relationship between the number of wires and sensitivity is observed not to be linear. The increase is not linear probably due to two possible reasons: 1) mounting amount in defects with increasing number wires; 2) inter-diffusion distance between the wires is relatively large. The enhancement will be much greater if the distance can be reduced to magnitude in the order of 10μm.

7. Conclusions

1) Theoretical analysis and modeling have been made on the magnetic behavior of a ferromagnetic wire array, from which the principles and guidelines for the design and development of composite ferromagnetic functional materials have been generated. The effective volume principle requires the ferromagnetic functional materials to be in insulated ferromagnetic wire array and the number of wires should be as many as possible for a certain volume of material, leading to a requirement of nanoscaled wires. The dynamic domain unification principle requires the ferromagnetic wires in an array to be intimately close to each other with insulation in between, leading to the requirement of nanoscaled array structure.
2) Nanoscale thickness stripe $Ni_{80}Fe_{20}$ arrays have been successfully synthesized using a combination of lithography and sputtering. However, due to the limitation of the sputtering machine, i.e. high sputtering pressure 10^{-6} and possible contaminations, the sputtered structures displayed poor sensitivity. A better sputtering system (lower sputtering pressure) has found and the work will be repeated using the better machine.
3) Template assisted electrodeposition was successfully implemented to develop arrays of $Ni_{80}Fe_{20}$ wires. This approach is limited by the technology for the fabrication of the template. Under the conditions in this project, the diameter of the holes drilled on the template was limited to micro scales and the aspect ratio was limited to 1:50.
4) Using a customized fixture to hold the wires in place, electrodeposition of multiple wires was successfully carried out to achieve the insulator/$Ni_{80}Fe_{20}$/Cu/ $Ni_{80}Fe_{20}$/insulator wire array. Sensitivity measurements showed that the sensitivity of the sensor with 4 wire array sensing element was at least 3 times more that that with single wire sensing element, confirming the effectiveness of the composite ferromagnetic functional materials.

8. Recommendations

In view of the limitations and fabrication difficulties with the approaches tested in this project for developing the nanostructured composite ferromagnetic functional materials that are especially useful to high sensitivity micro sensors for weak magnetic field, a better approach is recommended, which is cold-drawing or cold-rolling. In this approach, a large number of insulator/$Ni_{80}Fe_{20}$/Cu/ $Ni_{80}Fe_{20}$/insulator rods are packed together to go through a series of cold-drawing or cold-rolling process. The process is repeated till the size scale of each rod in the pack down to micro or nanometer levels as required. This approach has all the advantages against the limitations of those tested in the present project.

List of Publications

From the results, two papers have to been written and submitted for international journal publication:

1) H.L. Seet, X.P. Li, M.H. Hong, K.S. Lee, K.H. Teh, H.H. Teo, "Electrodeposition of Ni-Fe Micro Pillars Using Laser Drilled Templates" *Journal of Materials Processing Technology*, In Press (2007)
2) H.L. Seet, X.P. Li, K.S. Lee, H.Y. Chia, "Nanocrystalline grain size of $Ni_{80}Fe_{20}$/Cu micro-composite wires by different electrodeposition methods" *Journal of Materials Processing Technology*, In Press (2007)

Two more papers, one on the magnetic behavior of ferromagnetic wire array, and another one on magnetic interactions of ferromagnetic wires in an array in relation to the frequency of the AC passing through the wire array, are in the process of writing for international journal publication.

References

[1] X.P. Li, H.L. Seet, J. Fan, J.B. Yi, "Electrodeposition and characteristics of $Ni_{80}Fe_{20}$/Cu composite wires", *Journal of Magnetism and Magnetic Materials* **304** (2006) 111-116.

[2] X.P. Li, Z.J. Zhao, S. Ang, S.J. Koh, T.B. Oh, J.Y. Lee, W.X. Chen, "Effect of the pH Value on the Magnetic Properties of Electroplated NiFe Layers", *Materials Science Forum* **437-438** (2003) 57-60.

[3] H.L. Seet, X.P. Li, N.Ning, W.C. Ng, J.B. Yi, "Effect of Magnetic Coating Layer Thickness on the Magnetic Properties of Electrodeposited NiFe/Cu Composite Wires", *IEEE Transactions on Magnetics* **42(10)** (2006) 2784-2786.

[4] J.B. Yi, X.P. Li, J. Ding, H.L. Seet, "Study of the grain size, particle size and roughness of substrate in relation to the magnetic properties of electroplated permalloy", *Journal of Alloys and Compounds* **428(1-2)** (2007) 230-236.

[5] X.P. Li, J. Fan, X.B. Qian, J. Ding, " Multi-core orthogonal fluxgate sensors", *Journal of Magnetism and Magnetic Materials* **300(1)** (2006) e98-e103.